Tellus (1999), 51A, 803–814
Printed in UK. All rights reserved

TELLUS
ISSN 0280–6495

Storm tracks in regional climate simulations: verification and changes with doubled CO_2

By J. J. KATZFEY, *CSIRO Atmospheric Research, Private Bag 1, Aspendale, Victoria, Australia 3195*

(Manuscript received 28 September 1998; in final form 29 March 1999)

ABSTRACT

The ability of the CSIRO Atmospheric Research's regional climate model (RCM) to simulate the mean July storm track over Australia is investigated in this study. The observed storm track is characterized by the time-averaged eddy kinetic energy in the ECMWF analyses for years 1985–1992. RCM runs nested within these analyses are used to verify the ability of the model to simulate the storm track with "perfect" boundary conditions. Comparison is also made with 20 years of the CSIRO9 Mk2 global climate model (GCM) and the RCM nested within this GCM, for equilibrium simulations with both current and doubled CO_2 levels. Correlations of the meridional wind with a point within the storm track over Australia are used to characterize the structure of the mean baroclinic wave within the storm track. The location of the storm tracks in both the RCM and the GCM are simulated very well. The main deficiency is the lack of intensity of the upper-level storm track, but the RCM is more realistic than the GCM, indicating that the intensity of the storm track is partly related to horizontal resolution. The mean wave structure in the GCM and the RCM simulations is very similar to observed. Under doubled CO_2 conditions, both the upper-level jetstream and storm track intensify, and move equatorward, in response to the increasing upper-troposphere north–south temperature gradient. In the lower troposphere, the mean and eddy kinetic energy decrease to the southeast of Australia in response to the decrease in the north–south temperature gradient there. As a response to the generally decreasing mid-tropospheric north–south temperature gradient, the mean baroclinic wave appears to become slightly more barotropic, as indicated by less tilt in the zonal direction.

1. Introduction

Regional climate models (RCMs) have been developed to more realistically simulate climate change with higher resolution for a limited domain (see summary by McGregor (1997)). In this study, the storm track and the baroclinic wave structure over Australia are investigated using eddy kinetic energy and correlation analysis applied to the European Centre for Medium-range Weather Forecasts (ECMWF) analyses and three RCM simulations: nested within the analyses, and within a GCM for both current and doubled CO_2 concentrations.

Several studies have investigated the impact of increasing greenhouse gases on cyclone activity. For example, Zhang and Wang (1997) investigated the winter cyclone and anticyclone activity in equilibrium global climate simulations of both current and future climates. By tracking cyclones and anticyclones and calculating 500 hPa height variability, they found that under greenhouse conditions cyclone activity in the northern winter decreased, which they associated with a weakening in the meridional temperature gradient and a reduction in the land–ocean contrast.

A summary of the characteristics of the storm

e-mail: jjk@dar.csiro.au

track in the southern hemisphere was presented by Trenberth (1991) using the ECMWF analyses. The storm track is usually defined as the region of maximum variance of the 500 hPa heights. It is closely related to the passage of highs and lows or troughs and ridges (Wallace et al., 1988). Trenberth's study focussed primarily on the mean zonal characteristics of the storm track and its relationship to the mean flow.

In order to determine the structure and evolution of the transient disturbances in the northern Pacific Ocean, Lim and Wallace (1991) completed a regression analysis of various fields to the 500 hPa heights. Their analysis found a structure that was suggestive of an evolving "generic" baroclinic wave. In a similar type of analysis, Berbery and Vera (1996) used correlation analysis of the meridional wind component to investigate the characteristics of the southern hemisphere winter storm track. They found that the unfiltered meridional wind component was adequate to represent the features of synoptic-scale eddies and also found indications of downstream development of the waves, especially in the subtropical jetstream.

In this study, the kinetic energy of the July flow is used to characterize the jetstreams while the kinetic energy of the eddies is used to determine the storm track. The use of the eddy kinetic energy gives similar results to the 500 hPa heights or the meridional wind in characterizing the storm track. Data used are from 8 Julys of the ECMWF analyses, a RCM nested within those Julys and 20 Julys of a GCM and corresponding nested RCM for both $1 \times CO_2$ and $2 \times CO_2$. These data are investigated to determine characteristics of the winter upper- and lower-level storm track over Australia, how well the models capture the storm track and possible changes with doubled CO_2. The next section describes the data and models used in this study. This is followed by analyses of the storm track in current climate conditions. In Section 4, the changes in the storm track under enhanced greenhouse conditions are investigated. The results are then summarized.

2. Data and model description

The ECMWF data used in this study are the standard 14 pressure-level analyses on a 2.5° by 2.5° latitude–longitude grid for years 1985–1992. A 16 point, bicubic Bessel procedure was used to horizontally interpolate the data to a Lambert-conformal grid. The surface topography was determined using the grid box average of all points of the 5 min US Navy topography data set. A 1–2–1 filter was applied to the interpolated topography data in both directions to eliminate $2\Delta x$ features. The surface pressure was then computed hydrostatically from the geopotential heights and temperatures of the analyses using the data at levels above and below the surface topography. Temperature and winds were then vertically interpolated using splines while the moisture was linearly interpolated, both using log pressure as the vertical coordinate. A dry adiabatic adjustment was also applied to the initial temperatures.

The GCM data used are from the nine level CSIRO9 Mk2 R21 equilibrium slab ocean global climate model (GCM) simulations (see Watterson et al., 1997 for discussion of the GCM results). 20 Julys from both the $1\times$ and $2 \times CO_2$ concentrations simulations are used.

The RCM used in this study is the CSIRO Division of Atmospheric Research Limited Area Model (DARLAM). It is a two-time-level, semi-implicit, hydrostatic primitive equations model with a comprehensive physics package. Brief model descriptions and results of earlier nested climate simulations are summarized in McGregor (1997). The model used in this study had nine vertical sigma levels for the 125 km horizontal resolution Lambert-conformal grid for domain shown in Fig. 1. One-way nesting with exponentially decreasing weights was applied at the lateral boundaries.

A large-scale nudging was also applied to the RCM fields of temperature, winds and surface pressure. At each time step of the RCM, an 11×11 point (about 1400 km × 1400 km) box average of the RCM and the GCM on the RCM grid was computed. The RCM box average was then relaxed back to the GCM box average every time step with a relaxation time of 96 h. Since only the box average was nudged, the smaller scale features were relatively unaffected. This was done to reduce the build-up of large-scale biases in the regional model compared to the boundary forcing. In mid-latitudes, this nudging had little effect, since the sufficient flow of boundary data into the domain prevented any significant RCM biases from developing. In the tropics however, the lack of signific-

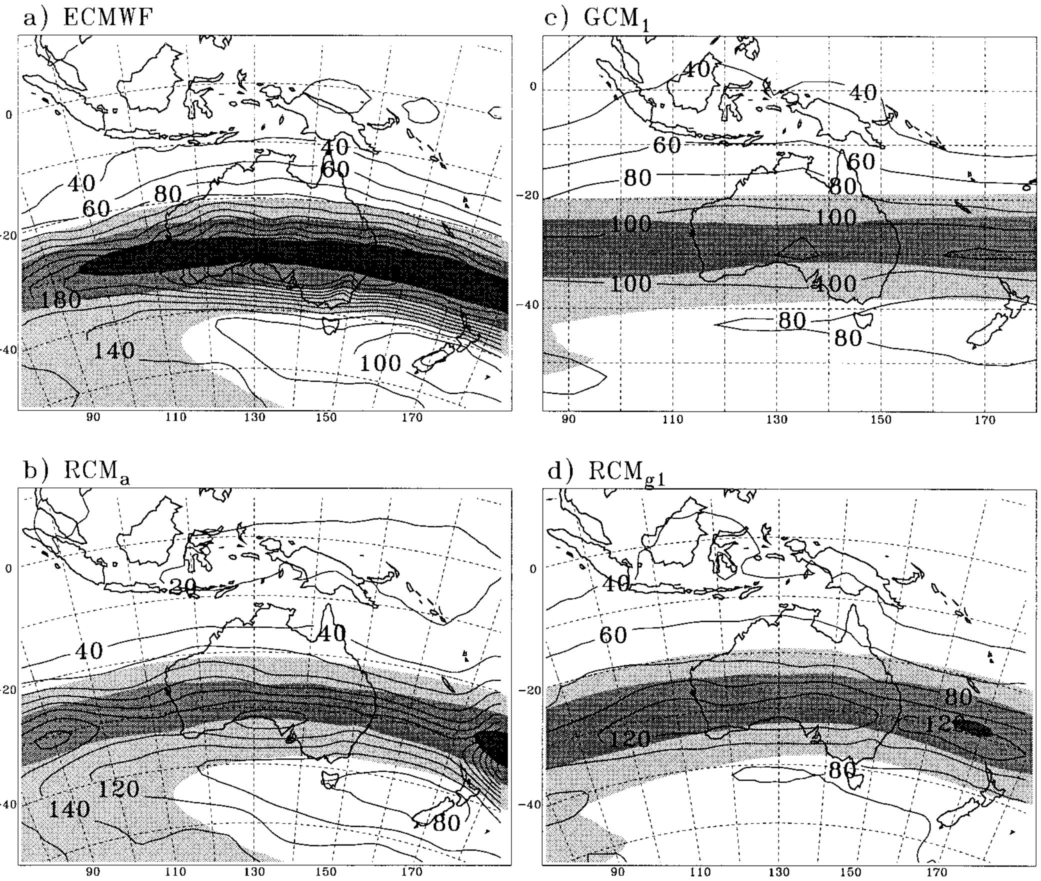

Fig. 1. July 200 hPa kinetic energy of the mean flow (shaded, every 500 $m^2 s^{-2}$) and eddy kinetic energy (solid contours every 20 $m^2 s^{-2}$) for (a) ECMWF analyses, (b) RCM_a, (c) GCM_1, (d) RCM_{g1}.

ant flow into the domain of boundary information allowed the RCM to develop biases which, because of the one-way nesting, cannot leave the model domain. The large scale nudging was found to be a useful technique to prevent significant biases developing in the tropics.

The RCM was nested within the ECMWF analyses for 8 Julys (1985–1992) in single month mode. The ECMWF analyses are provided every 12 h and were linearly interpolated in time. The RCM was also nested within the GCM for 20 years in continuous mode, meaning the model was initialized with the GCM data at the start of the run and then only sea surface temperatures (SST) and lateral boundary data from the GCM were specified, apart from the large-scale nudging. The GCM boundary and SST data were provided every 8 h and were linearly interpolated in time.

In this study, the kinetic energy is used to characterize the magnitude and the location of the jetstreams. The eddy kinetic energy is used to characterize the storm track and will measure the amount of energy associated with the transient weather systems. Only averages for July (southern hemisphere winter) are presented here since this is when the storm track associated with the subtropical jet lies above the Australian continent. The unfiltered winds are used in this study since Berbery and Vera (1996) found that this was adequate to characterize the southern hemisphere winter storm track and in order to simplify the computations.

3. Storm tracks in the current climate

In order to determine the location and intensity of the upper-level jetstream and storm track, the mean of all available July 200 hPa total kinetic energies (KE) and kinetic energy of the eddies (EKE) are presented in Fig. 1 (shading) for: ECMWF analyses (Fig. 1a), RCM nested within analyses (RCM_a, Fig. 1b), the CSIRO9 GCM at $1 \times CO_2$ (GCM_1, Fig. 1c) and the RCM nested within CSIRO9 GCM at $1 \times CO_2$ (RCM_{g1}, Fig. 1d). The subtropical jetstream is evident over the Australian continent in July with a maximum of KE in the analyses of over $1500\,m^2\,s^{-2}$. In general, RCM_a underpredicts the peak KE in the jetstream by about $500\,m^2\,s^{-2}$ (about 30%), but its location is generally good. Note that with the boundary forcing, the KE at the boundaries matches that of the analyses, but does not show the increase (and even has slight decreases) of KE over the Australian continent. The KE in GCM_1 is similar to, but slightly less than, RCM_a. Again, there is a slight decrease in KE over Australia, in contrast to the analyses. Finally, the KE of the RCM_{g1} is slightly greater than in GCM_1 and RCM_a, although still less than the analysis. The larger values in RCM_{g1} compared with the GCM_1 indicates that the increased resolution of the RCM causes an increase in KE, although still not up to the level in the analyses.

The 200 hPa EKE (contours in Fig. 1) in the analyses has a maximum of over $320\,m^2\,s^{-2}$ (nearly 20% of the KE) just poleward of the KE maximum, which is consistent with the results of Trenberth (1991). There is a slight hint of greater EKE (and KE) along the southern boundary, which is related to the polar jet and its associated storm track. The RCM_a significantly underpredicts the EKE, with peak values over Australia of only $160\,m^2\,s^{-2}$ (about half of the observed values). The GCM_1 has even less EKE, with peak values of around $120\,m^2\,s^{-2}$. The RCM_{g1} again has more EKE than the GCM, although still less than RCM_a and the analyses. The EKE for RCM_{g1} is less than RCM_a, even though the KE was slightly larger, implying an influence of the eddies coming through the lateral boundaries from the GCM. These results suggest that the total kinetic energy is only slightly improved by horizontal resolution, while the eddy kinetic energy is influenced by both horizontal resolution and the eddy kinetic energy specified at the lateral boundaries.

The upper-level KE is a measure of the jetstream while the EKE is a measure of the strength of the jet streaks and waves in the upper troposphere. However, it is also of interest to investigate the strength of the flow and eddies in the low troposphere which are more closely linked to the transient weather producing systems (highs and lows). To this end, the KE and EKE at 900 hPa are shown in Fig. 2 for the same data sets. The overall pattern in all datasets is a maximum of KE over the ocean south of Australia (over $150\,m^2\,s^{-2}$ for ECMWF). This region is where there are strong westerlies between the subtropical highs (located over Australia) and the polar trough at the periphery of Antarctica. There is also a smaller maximum of KE to the north of Australia (about $50\,m^2\,s^{-2}$ for ECMWF) associated with the dry, wintertime southeasterly trade winds. All models capture these features, although the models tend to overpredict the strength of the trade winds (greater than $75\,m^2\,s^{-2}$ KE for all models) when compared with the analyses. One possible source of the difference between the analysis and the models is the ECMWF data was interpolated from the 1000 and 850 hPa data to the sigma surface near 900 hPa, which might cause the magnitudes in to be lower than for the models. South of Australia, the RCM_a predicts KE amounts very similar (and even slightly greater) than in the analyses. The GCM and RCM_{g1} underpredict the magnitude of KE south of Australia, primarily due to the lack of the meridional component of KE (not shown). There is very little difference in KE between these two models at this level, apart from a slightly greater KE in RCM_{g1} along and to the east of the east coast of Australia. This feature is more similar to the analyses (and RCM_a) and suggests that RCM_{g1} is capturing this feature better than the GCM.

The low-level storm track, as measured by the EKE and shown as contours in Fig. 2, is located along the southern boundary with a maximum in the southwestern corner of the domain. The RCM_a has very similar values of EKE compared with the analysis. The GCM_1 has greater values of EKE than either the analyses or RCM_a south of Australia, but has less EKE east of Australia (note location of $40\,m^2\,s^{-2}$ contour). RCM_{g1} predicts slightly lesser amounts of EKE compared to the

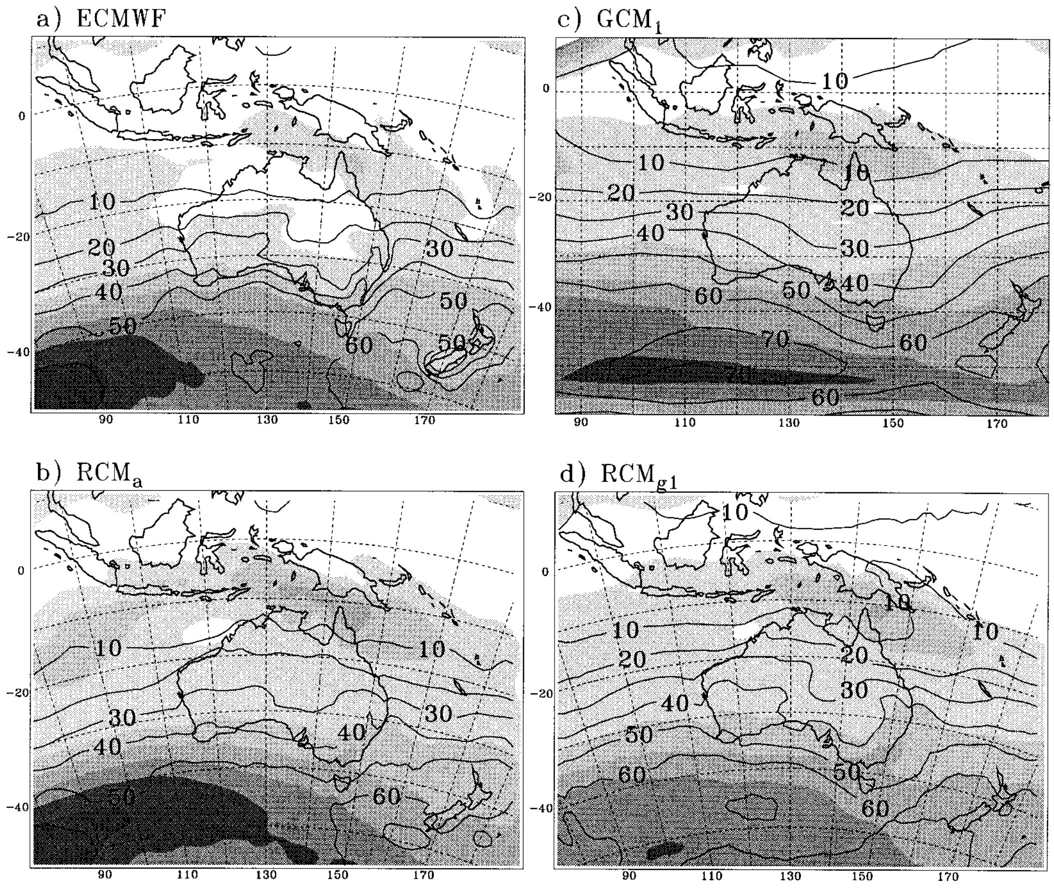

Fig. 2. July 900 hPa kinetic energy of the mean flow (shaded, every 25 $m^2 s^{-2}$) and eddy kinetic energy (solid contours every 10 $m^2 s^{-2}$) for (a) ECMWF analyses, (b) RCM_a, (c) GCM_1, (d) RCM_{g1}.

GCM_1, but still more than the analyses and RCM_a. Note that just east of Australia, there is an increase of EKE in the analysis, RCM_a and RCM_{g1} (to greater than 40 $m^2 s^{-2}$), while the GCM shows increases further east. Evidently, the GCM does not develop eddies immediately downstream of Australia as is apparent in the analysis and the RCM.

In order to assess the realism of the wave structure in the models, correlations of the 200 hPa meridional wind with a base point within the storm track at 31°S, 130°E were computed, similar to Berbery and Vera (1996). The averaged results for all Julys in the respective simulations are shown in Fig. 3. The correlations for the analysis show about a two-wave structure within the model domain. The wavelength of this "mean" wave is about 4800 km, similar to the results of Berbery and Vera (1996). There is also a hint that the waves start at the poleward side of the subtropical jetstream west of Australia and then propagate along the jetstream axis over Australia, again consistent with Berbery and Vera, who found a split of the waves west of Australia, with one branch propagating along the subtropical jetstream over Australia and the other along the polar jetstream. The structures of the baroclinic waves in the RCM and GCM simulations are very similar to those in the analysis, indicating that the simulated wave structure in the model is realistic. The RCM simulations show slightly greater negative correlations along both Australian coasts compared with the corresponding boundary data fields, possibly indicating more coherent/stronger

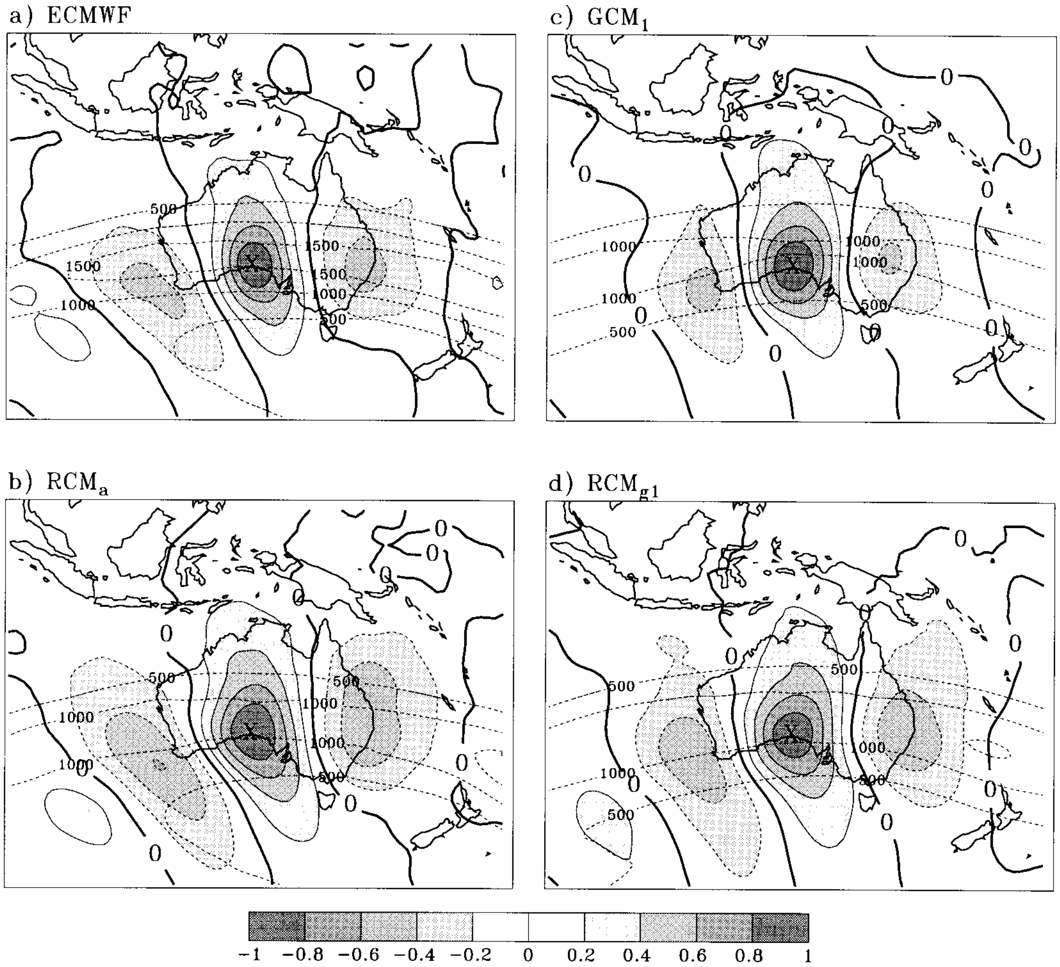

Fig. 3. Mean correlations of the 200 10 hPa meridional wind with the wind at 31°S, 130°E and 200 hPa (marked with "X") for (a) ECMWF analyses, (b) RCM_a, (c) GCM_1, (d) RCM_{g1}. The kinetic energy is also indicated (dashed contours every 500 $m^2 s^{-2}$).

waves than in the analyses or the GCM. It is also interesting to note that the correlations have such a large meridional extent in all data sets, although the correlations at the northern and southern extremes are quite small.

4. Changes in storm tracks with doubled CO_2

The changes in the upper and lower storm tracks with doubled CO_2 for both the GCM and the RCM are now investigated. The GCM_2 was integrated with doubled CO_2 concentrations (660 ppmv) until equilibrium (Watterson et al., 1997; Whetton et al., 1996) and the RCM_{g2} was then nested within 20 years of this GCM simulation.

The upper-level (200 hPa) KE in the doubled CO_2 GCM and RCM simulations (Fig. 4a,b) has increased along the axis of the jetstream by over 200 $m^2 s^{-2}$ to the east and west of Australia and over 100 $m^2 s^{-2}$ over Australia, about a 10–15% increase in KE. Using a standard *t*-test, the shaded changes are statistically significant at the 99% level. The RCM_{g2} has slightly greater increases than the GCM_2 over Australia (increases of over

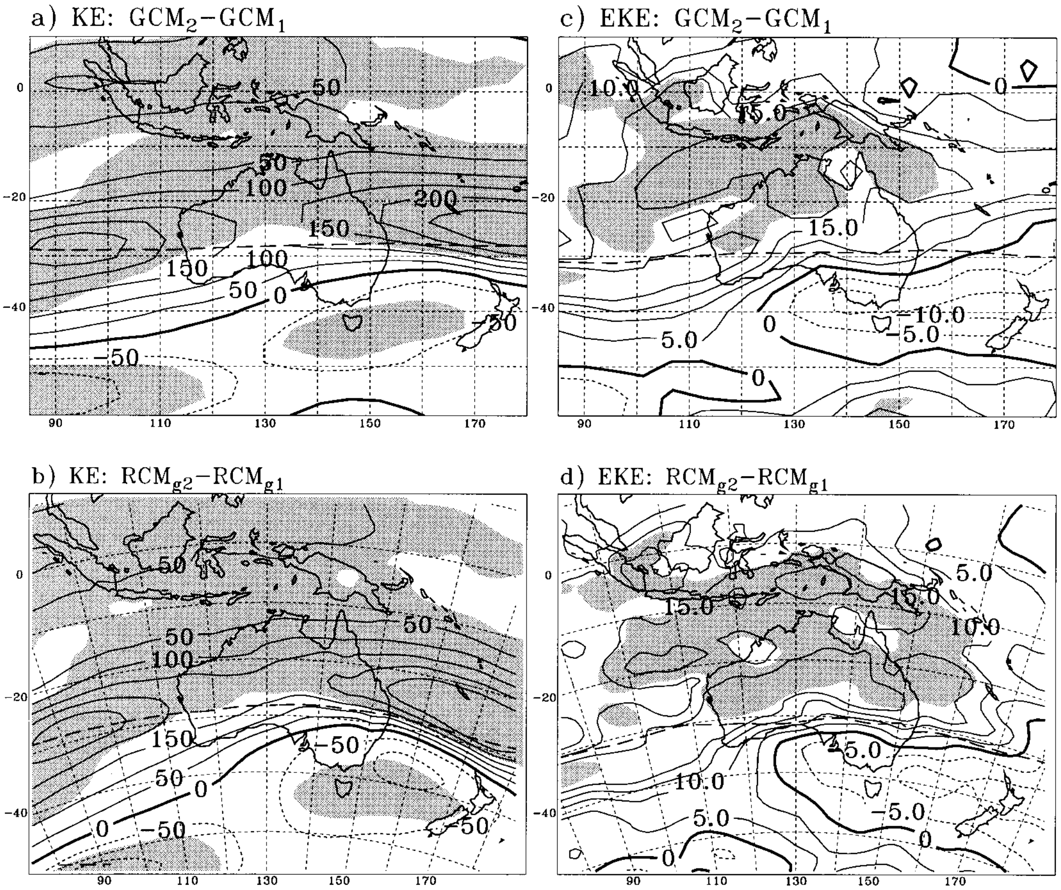

Fig. 4. July 200 hPa kinetic energy change $2 \times CO_2$–$1 \times CO_2$ (solid contours every $50\ m^2\ s^{-2}$) (a and b) and eddy kinetic energy change $2 \times CO_2$–$1 \times CO_2$ (solid contours every $5\ m^2\ s^{-2}$) (c and d) for GCM (a and c), and RCM (b and d). Shading is regions where changes is statistically significant at the 99% level. The long dash line is the axis of maximum kinetic energy (a and b) and maximum eddy kinetic energy (c and d).

$150\ m^2\ s^{-2}$). There is also a hint that the storm track to the east of Australia has shifted slightly equatorward in both models, since the increases are maximized north of the maximum KE. The only region of small KE decreases is south of Australia, poleward of the KE maximum. Even some of these smaller changes are significant at the 99% level.

The 200 hPa EKE also increases in both the GCM_2 and the RCM_{g2} over most of Australia by about 15–$20\ m^2\ s^{-2}$, which is about a 15% increase. Again, these increases are statistically significant at the 99% level over northern Australia. As with the KE, there are slight decreases south of Australia and especially over New Zealand, but these changes are not statistically significant.

At 900 hPa (Fig. 5), the KE shows a general pattern of decrease, apart from the region of maximum KE to the southwest of Australia which shifts northward and increases in intensity. Over the Tasman Sea, to the southeast of Australia, the KE decreases by more than $15\ m^2\ s^{-2}$, most of which is statistically significant at the 99% level.

The EKE shows similar decreases generally everywhere on the order of $-5\ m^2\ s^{-2}$. Larger decreases of more than $-15\ m^2\ s^{-2}$ (about a 20% decrease) occur in the RCM over the east of Australia, while in the GCM the decreases are about -5 to $-10\ m^2\ s^{-2}$. The decreases east of

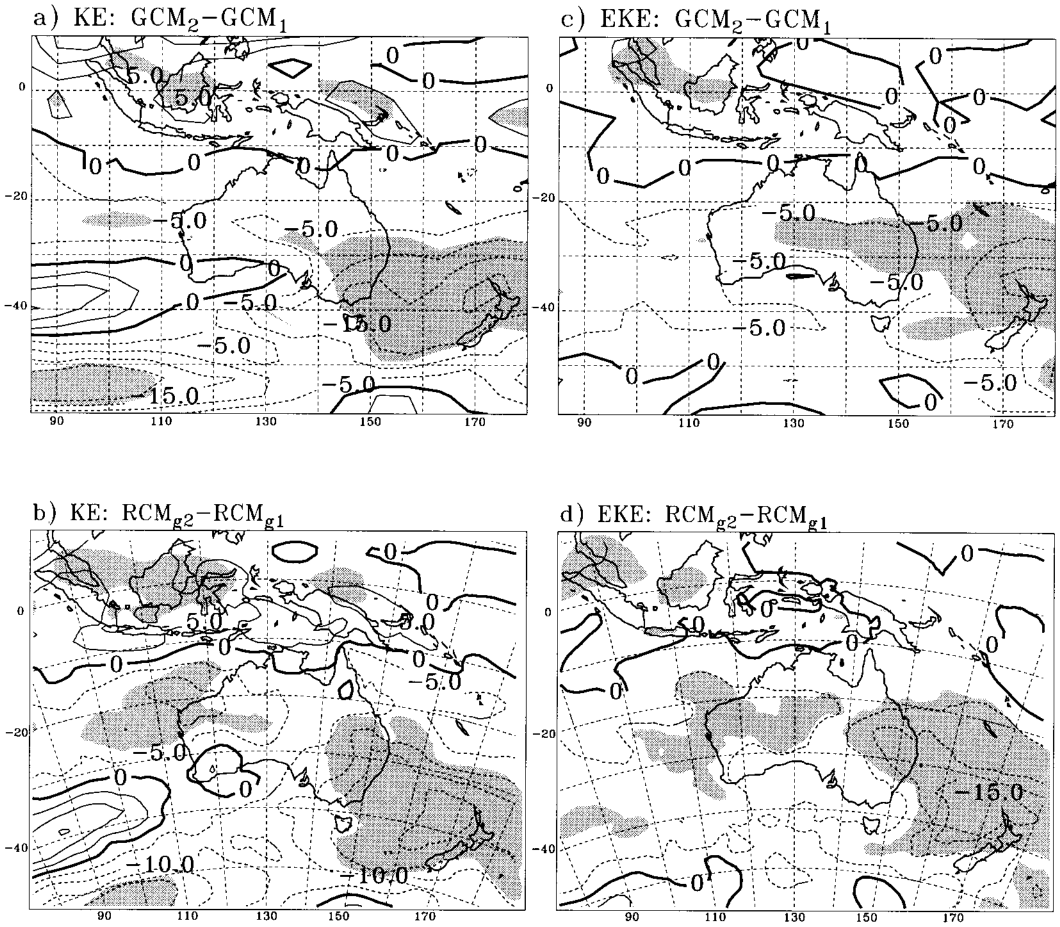

Fig. 5. July 900 hPa kinetic energy change $2 \times CO_2$–$1 \times CO_2$ (solid contours every $5\ m^2\ s^{-2}$) (a and b) and eddy kinetic energy change $2 \times CO_2$–$1 \times CO_2$ (solid contours every $5\ m^2\ s^{-2}$) (c and d) for GCM (a and c), and RCM (b and d). Shading is regions where changes is statistically significant at the 99% level.

Australia in both models are statistically significant at the 99% confidence level. The RCM changes in EKE at 900 hPa are only slightly smaller than the KE decreases indicating that the KE of the mean flow only decreases slightly (about $-5\ m^2\ s^{-2}$). The GCM EKE decreases of about $-5\ m^2\ s^{-2}$ are smaller in magnitude, while the KE decreases are of the order of $-15\ m^2\ s^{-2}$, indicating larger decreases in the KE of the mean flow in the GCM. Note that although the KE increases to the southwest of Australia, the EKE decreases slightly, implying an increase in the KE of the mean flow.

In summary, there are statistically significant increases in both KE and EKE in upper-levels within the jetstream. Some decreases occur further south as the jetstream shifts equatorward. At low-levels, there is a statistically significant decrease in KE and EKE over the Tasman Sea between Australia and New Zealand. It is interesting to note that the change in mean kinetic energy over the Tasman Sea in the GCM_2 is larger than the EKE, while the reverse is true for the RCM_{g2} with the EKE decreases nearly three times as large as for the KE of the mean flow. Thus, the character of the change in kinetic energy is different in the GCM and the RCM in this region. Although the changes in total KE are generally similar, the changes in EKE are different in magnitude. The fact that the RCM better simulates the EKE

(Fig. 2) suggests the RCM changes might be more believable.

In order to further elucidate the vertical structure of the KE and EKE and their changes, July north–south vertical cross-sections averaged over the Australian continent are presented in Fig. 6. The KE shows the subtropical jetstream is located over Australia at about 200 hPa with a peak value of over 1200 $m^2 s^{-2}$. There is also evidence of the polar stratospheric wintertime jet to the south. The eddy kinetic energy has four maxima: one associated with the subtropical jet over Australia at 200 hPa (maximum about 120 $m^2 s^{-2}$), one at 350 hPa further south (maximum 140 $m^2 s^{-2}$), one connected with the polar stratospheric jet, and the final maximum of over 60 $m^2 s^{-2}$ in the low troposphere south of Australia. In the study of Trenberth (1991), these separate maxima were not apparent, although only zonal mean cross-sections were presented in that paper.

The changes in KE associated with enhanced greenhouse conditions (Fig. 6b) show the upper-level KE increases are confined to above about 300 hPa over Australia and extend into the stratosphere further south. There are decreases in KE of about -50 $m^2 s^{-2}$ at around 500 hPa below

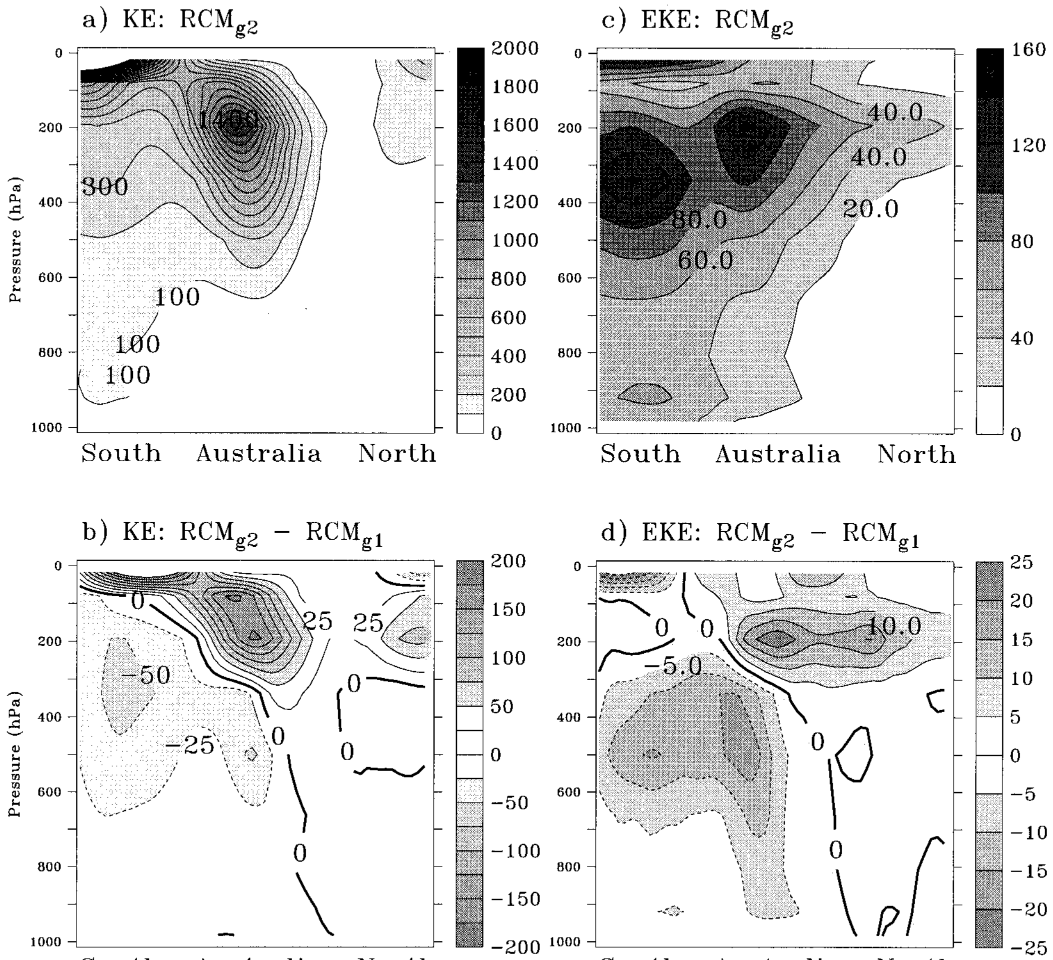

Fig. 6. July south–north vertical cross-section of RCM: (a) kinetic energy (every 100 $m^2 s^{-2}$), (b) kinetic energy change 2 × CO_2–1 × CO_2 (contours every 25 $m^2 s^{-2}$), (c) eddy kinetic energy (every 20 $m^2 s^{-2}$), and (d) eddy kinetic energy change 2 × CO_2–1 × CO_2 (contours every 5 $m^2 s^{-2}$).

the subtropical jetstream over Australia and KE decreases throughout the troposphere in more southern latitudes, with peak decreases over $-50\ m^2\ s^{-2}$ located in the upper troposphere.

The changes in EKE with doubled CO_2 (Fig. 6d) show a dipole pattern with decreases in the mid- to low troposphere over Australia and further south and increases in the upper troposphere over Australia. In general, the storm track associated with the subtropical jetstream increases in upper levels, while the polar and low-level storm tracks decrease in intensity.

To help understand why these changes are occurring, the potential temperature and the meridional circulation for the same July mean cross-section are presented in Fig. 7a while their changes with doubled CO_2 are shown in Fig. 7b. It is clearly evident that the tropopause in the model is at the sigma level near 200 hPa, which is similar to that from the ECMWF analyses when interpolated to the same 9 sigma levels (not shown). The mid tropospheric north–south temperature gradient associated with the subtropical jetstream is evident over Australia. The meridional circulation is indicated by vectors using the meridional wind as the horizontal component and the vertical component is minus five times the vertical velocity (ω in μb/s). Note the general subsidence over Australia in the middle of the cross-section associated with sub-tropical highs and the descending branch of the Hadley circulation. The rising branch of the Hadley circulation is evident in the tropical north, although the simulation tends not to have this ascent extend to the tropopause, as in the analyses (not shown).

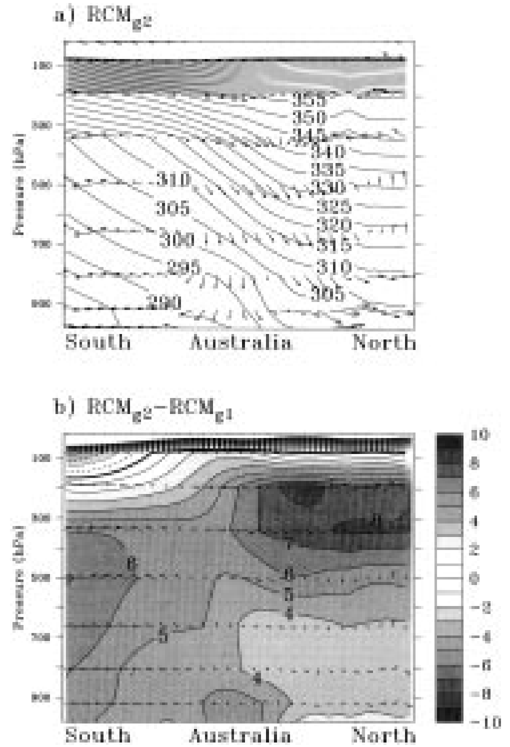

Fig. 7. July south–north vertical cross-section of RCM: (a) $1 \times CO_2$ potential temperature (contours, every 5 K) and meridional circulation (v wind in the horizontal and $-5^*\omega$ in the vertical) and (b) $2 \times CO_2$–$1 \times CO_2$ change in potential temperature (contours, every 1 K) and meridional circulation.

The temperature changes indicated in Fig. 7b show strong warming (about 8°C) in the upper tropical troposphere and warming of over 6°C in the more poleward middle troposphere. The model also simulates cooling in the stratosphere. Note that the greatest warming near the surface is for more poleward latitudes. The changes in the meridional circulation are slight, with a suggestion of an enhancement of the Hadley circulation (slightly greater ascent and descent, also slightly deeper circulation) and more poleward flow further south.

The main effect of the tropospheric temperature changes is to decrease the north–south temperature gradient throughout the lower half of the troposphere, causing a weakening of the mid-tropospheric winds (and KE) in this region through thermal wind considerations. However, above 400 hPa, the north–south temperature gradient is increased, giving rise to stronger upper troposphere jets and KE. The increase in upper tropospheric EKE results because of the greater available potential energy (associated with the greater temperature contrast) and greater mean KE available for the eddies. Conversely, the decreases in the north–south temperature gradient throughout the middle to lower troposphere, especially in more southern latitudes, is associated with the decrease in the KE and EKE. In addition, the increased vertical dry static stability will lead to greater decoupling of the upper- and lower-level baroclinic waves. If one assumes that the upper-level waves provide one of the forcing mechanisms for the development of the low-level systems, this decoupling can lead to weaker low-level systems. However, the increase in low-level EKE to the southwest of Australia is related to a decrease in vertical stability, associated with greater warming in the lower troposphere (not shown), thereby allowing the greater interaction of the upper jetstream with the surface causing increased low-level KE and EKE (Fig. 5).

In order to investigate the changes in the baroclinic wave structure that are associated with doubled CO_2, the July west–east cross-sections over Australia of the correlations of the meridional wind to the point 31°S, 130°E and 200 hPa for $1 \times CO_2$ and its change with $2 \times CO_2$ are shown in Fig. 8. The correlations show the expected tilt of the baroclinic waves to the west with height in the model. The changes with doubled CO_2 show generally reduced correlations at lower levels and a decrease in vertical tilt indicating that the waves are becoming more barotropic, especially in the lower troposphere. These results are in agreement with the decreased meridional temperature gradients noted in Fig. 7b and the decoupling of the upper- and lower-level systems discussed before.

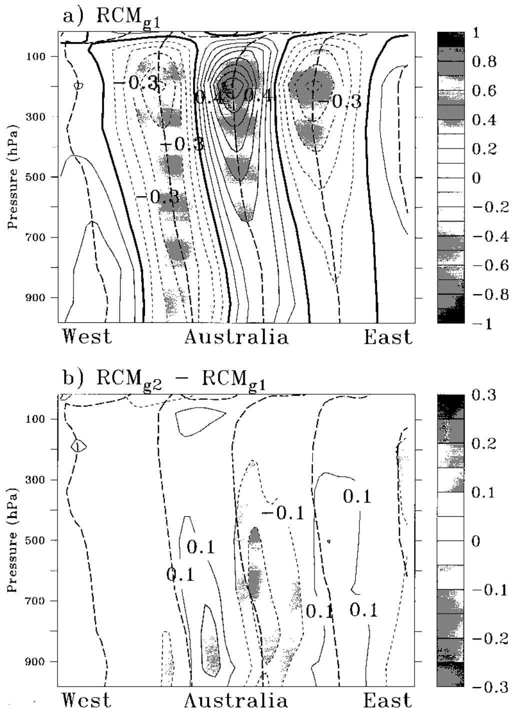

Fig. 8. July west–east vertical cross-section of mean correlations of the meridional wind with base point at 31°S, 130°E and 200 hPa for RCM: (a) $1 \times CO_1$ (contour every 0.1) and (b) correlation change $2 \times CO_2$–$1 \times CO_2$ (contour every 0.1, but not 0). Thick unlabeled dashed line is axis of maximum/minimum correlations in the $1 \times CO_1$ simulation (a).

5. Conclusions

In this study, the storm tracks for the Australian region in the current climate for a regional climate model and a global climate model are verified against 8 years of ECMWF analyses for July. The GCM data used were from 20 Julys of an equilibrium, slab-ocean, R21, nine level CSIRO Mk2 simulation. The 125 km, nine level RCM data came from runs nested within both the 8 Julys of the analyses and the 20 years of the GCM simulation in seasonal mode. In addition, The GCM and RCM were run with doubled CO_2 to investigate the potential changes under enhanced greenhouse conditions. Only results from July were presented here.

In summary, the RCM and GCM accurately predict the location of the upper-level storm track over Australia. However, they both underpredict the magnitude of the upper-level kinetic energy (KE) and storm track (EKE). The RCM nested within the analyses had the best representation of the EKE, though still only about half the magnitude of the analyses. The RCM nested within the GCM has greater KE and EKE compared with the GCM, closer to the analyses, suggesting that the RCM can improve upon the GCM for the intensity of the storm track. These results suggest that the amount of KE and EKE in the RCM are dependent upon the model resolution (RCM_g versus GCM) and lateral boundary conditions (RCM_a versus RCM_g). Understanding why the RCM (and GCM) have weak upper tropospheric KE and EKE when compared to the analyses, even when nested within these analyses, requires further study.

Both the low-level KE and EKE are much more realistic in all simulations, but with some excessive KE to the south of Australia in the GCM also persisting in the RCM, although this may be due to the differing number of years (8 for analyses versus 20 for the GCM). East of Australia, the RCM improves upon the GCM for both the KE and EKE.

Correlations of the meridional wind with a point located at 200 hPa within the storm track over Australia were computed in order to determine the "mean" baroclinic wave structure of the simulations. All models captured the baroclinic wave structure very well, both in wavelength and pattern of the correlation.

The doubled CO_2 simulations showed increased upper-level KE and storm track intensity (EKE) and a slight shift equatorward of the maximum of both to the east of Australia. At low-levels, the KE decreased significantly to the south and southeast of Australia and slightly intensified and shifted equatorward to the southwest of Australia. The EKE generally decreased over Australia, and especially to the southeast over the Tasman Sea. These changes in KE and EKE were related to the increase in north–south temperature in the upper troposphere and decrease in the middle to lower troposphere. These results are in general agreement with Katzfey and McInnes (1996) who showed a general decrease in the number of Australian cutoff lows in the Tasman Sea with enhanced greenhouse. A more thorough investigation of the relationship of the low pressure systems and the eddy kinetic energy is planned.

Changes in the meridional wind correlations suggest that the waves are becoming weaker and more barotropic. This is consistent with the decoupling of the upper and lower wave activity and the decrease in the north–south temperature gradient.

One caveat of these climate change results is the use of equilibrium, slab–ocean GCM simulations as boundary data. These simulations tend to have larger temperature changes compared with coupled model results at $2 \times CO_2$ and the lower tropospheric temperature gradient changes in the southern hemisphere can be reversed in the coupled model results due to the slower warming of the polar oceans (Whetton et al., 1996). Recently, a 140 year regional climate simulation has been completed using DARLAM nested within the CSIRO9 transient coupled GCM. Preliminary analysis suggests the upper-level changes are generally similar, but the low-level EKE decreases east of Australia become increases. Analysis of this run is the subject of current research.

This study is the first application of the correlation technique to a regional climate model to investigate changes with doubled CO_2. Future work will investigate the changes in the dynamics, thermodynamics and energetics of the waves. In addition, further investigation of applying the correlation (or regression) technique to relate the upper-level wave to other fields, such as clouds, precipitation and low pressure systems, will be undertaken.

6. Acknowledgements

The author wishes to thank John McGregor and Kim Nguyen for help in setting up and running DARLAM. The project forms a part of the CSIRO Climate Change Research Program and has been funded in part by the Australian Department of the Environment, Sport and Territories. The author also wishes to thank the developers and maintainers of the FERRET graphics and analysis program.

REFERENCES

Berbery, E. H. and Vera, C. S. 1996. Characteristics of the Southern Hemisphere winter storm track with filtered and unfiltered data. *J. Atmos. Sci.* **53**, 468–481.

Katzfey, J. J. and McInnes, K. L. 1996. GCM simulations of eastern Australian cutoff lows. *J. Clim.* **9**, 2337–2355.

Lim, G.-H. and Wallace, J. M. 1991. Structure and evolution of baroclinic waves as inferred from regression analysis. *J. Atmos. Sci.* **48**, 1718–1731.

McGregor, J. L. 1997: Regional climate modelling. *Meteor. Atmos. Phys.* **63**, 105–117.

Trenberth, K. E. 1991. Storm tracks in the Southern Hemisphere. *J. Atmos. Sci.* **48**, 2159–2178.

Wallace, J. H., Lim, G.-H. and Blackmon, M. L. 1988. Relationship between cyclone tracks, anticyclone tracks, and baroclinic waveguides. *J. Atmos. Sci.* **45**, 439–462.

Watterson, I. G., O'Farrell, S. P. and Dix, M. R. 1997. Energy transports in climates simulated by a model which includes dynamic sea ice. *J. Geophys. Res.* **102**, 11027–11037.

Whetton, P. H., England, M. H., O'Farrell, S. P., Watterson, I. G. and Pittock, A. B. 1996. Global comparison of the regional rainfall results of enhanced greenhouse coupled and mixed layer ocean experiments: Implications for climate change scenario development. *Clim. Change* **33**, 497–519.

Zhang, Y. and Wang, W.-C. 1997: Model-simulated Northern winter cyclone and anticyclone activity under a greenhouse warming scenario. *J. Clim.* **10**, 1616–1634.